Guided Lamb waves in reconfigurable phononic crystal waveguides

Yan-Feng Wang,[1] Li Yang,[2] Ting-Ting Wang,[3] A-Li Chen,[2] Vincent Laude,[4, a)] and Yue-Sheng Wang[1, 2, b)]
[1)] *School of Mechanical Engineering, Tianjin University, Tianjin 300350, China*
[2)] *Institute of Engineering Mechanics, Beijing Jiaotong University, Beijing 100044, China*
[3)] *School of Mechanics, Civil Engineering and Architecture, Northwestern Polytechnical University, Xi'an 710129, China*
[4)] *Institut FEMTO-ST, CNRS, Univ. Bourgogne Franche-Comté, Besançon 25030, France*

We demonstrate experimentally the manipulation of Lamb waves guided along reconfigurable phononic circuits created by defects composed of threaded rods held with nuts in a perforated solid phononic crystal slab. Adjusting the free length of the rod, the resonant frequency of the defect can be tuned, without any change in the supporting phononic crystal slab. Both straight and bent waveguides are fabricated and measured in an aluminum sample with a lattice constant of 20 mm and a complete band gap extending from 50 to 70 kHz. Guidance of Lamb waves is clearly observed by Doppler vibrometer, even after 90° bends. The eigenmodes of guided waves are obtained using finite element analysis and to explain the tuning of resonances through a bending cantilever model. Numerical and experimental results are generally found to be in fair agreement. They also suggest that the guiding frequency is rather independent of the details of the waveguides. They are of significance for the design of reconfigurable phononic devices.

I. INTRODUCTION

Phononic crystals (PCs) are functional composites with spatial periodicity[1]. Their unique property is to exhibit band gaps in certain frequency range, within which propagation of elastic waves is prohibited. Thus, they have direct applications in noise isolation and vibration reduction[2]. When periodicity is broken, confined defect modes appear. Phononic crystals are a basis on which to design novel elastic wave devices such as waveguides[3], splitters[4], or acoustic channel drop filters[5]. Moreover, their dispersive properties in passing bands also result in promising phenomena, such as collimation or negative refraction[6].

Although phononic crystals provide a promising pathway to the manipulation of elastic waves, there have had few real-life applications so far. Actually, most of them are characterized by a passive response and operate in fixed frequency ranges. The topology or the material parameters are hardly tunable or reconfigurable after fabrication. Tunable manipulation of acoustic or elastic waves has thus become a fast developing topic[7]. Since elastic wave propagation is controlled mainly by material properties and geometry parameters[8], wave manipulation can generally be classified as based on either tunability or reconfigurability.

For tunable PCs, physical or material properties are tuned using an external control field. Such PCs may be composed of multiphysical coupled components, such as piezoelectric[9], ferroelectric[10], or magnetoelastic[11] materials. Dynamic control can be realized by applying an external biased electric field[12], a magnetic field[13,14], and so on. Piezoelectric materials are commonly used[15] and can be implemented either on the surface of or inside PC units. The resonance or Bragg scattering characteristics of the periodic structure can be tuned by an external circuit, so as to dynamically regulate wave propagation. When a feedback electronic control circuit is added[16], active or even smart control of wave propagation can be expected. Moreover, the response can self adapt to changes in the surrounding environment, such as an incident aerodynamic flow[17].

For reconfigurable PCs, the geometry or the layout is changed in a mechanical way. For instance, tunable manipulation can be realized continuously based on the reconfigurability of fluid/solid systems: rotating or removing the solid scatterers in a fluid matrix[3,18], or filling in a fluid in a solid matrix containing cavities[19–21]. Soft materials can also exhibit large deformations[22,23], so that their geometry or even topology can be changed owing to the bulking instability[24,25], leading to a significant change of wave dispersion. Thermal expansion of a solid material can also be used to control wave propagation to a certain extent[26]. Bistable or multi steady states of shape memory materials, including shape memory alloys[27] and polymers, can be used for the conversion of different wave characteristics.

Recently, PC slabs have received increasing interest for the manipulation of Lamb waves[20,28–30]. Investigations are focused on flat slabs decorated with holes[31] or solid inclusions[32], or grafted with pillars[33] or resonators[34]. Various devices, such as waveguides[35], splitters[36] and filters[37], have been designed and verified experimentally. However, manipulation of Lamb waves remains a difficult task[20]. In the present work, we demonstrate experimentally a simple way to reconfigure easily waveguides in

[a)] Electronic mail: vincent.laude@femto-st.fr
[b)] Electronic mail: yswang@tju.edu.cn

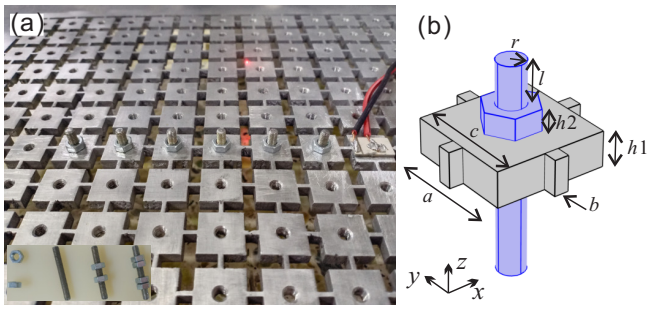

Figure 1. (a) Photograph of the phononic crystal slab sample. A linear waveguide is formed by a sequence of threaded rods clamped with nuts to the perforated square lumps. The inset is a close-up view of the rods and nuts used. (b) Unit cell of the phononic crystal slab and definition of geometrical dimensions.

perforated PC slabs. Threaded rods, held in dry mechanical contact with the slab using nuts, are added at chosen holes. Adjusting the free length of the rods, the resonance frequency of bending modes of the rods can be adjusted continuously within the complete phononic band gap. Straight waveguides and 90° bent coupled-resonator waveguides are formed experimentally in an aluminum PC slab. To explore the physical mechanism behind waveguiding, numerical simulations by using finite element analysis are performed. Numerical and experimental results generally agree fairly well, with slight frequency shifts of resonances. This work is of significance for the design of reconfigurable elastic wave devices.

II. EXPERIMENTAL AND NUMERICAL METHODS

The manufactured square-lattice phononic crystal slab sample is shown in Figure 1(a). It is machined in an aluminum plate. It consists of perforated square lumps connected by thin bars. In finite element computations, aluminum is considered isotropic (mass density $\rho_s = 2700$ kg/m^3, Poisson's ratio $\upsilon = 0.33$, and Young's modulus $E = 6.89$ GPa). The lattice constant is $a = 20$ mm and the thickness of the slab is $h_1 = a/4$. The width of the perforated square lumps is $c = 0.8a$ and the width of the connecting bar is $b = 0.1a$. The radius of the central hole is $r = 0.1a$. With those values, the phononic crystal slab possesses a wide complete phononic band gap, as Figure 2 shows (see Section III for a discussion).

Reconfigurability is implemented by the addition of threaded steel rods inside selected holes of the phononic crystal slab. The rods are clamped to the lumps by steel nuts placed symmetrically. In numerical computations, steel is considered isotropic (mass density $\rho_s = 6750$ kg/m^3, Poisson's ratio $\upsilon = 0.3$, and Young's modulus $E = 206$ GPa). The thickness of the nuts is $h_2 = 0.15a$. The total length of the rods is $L = 1.5a$ and their radius is $r = 0.1a$. As discussed in Section III, the length from nut to free end of a rod defines its resonance frequencies. By symmetry, we need only consider the length l of the rod above the plate (see Fig. 1b). The length of the rod below the plate is $L - h_1 - 2h_2 - l$.

Lamb waves are excited via a piezoelectric patch. Propagating Lamb waves are detected and imaged using a Polytec PSV-500 scanning vibrometer. Harmonic signals with either stepped or fixed frequencies are chosen for the measurement of transmission and displacement distribution, respectively. The excitation signal is amplified before it is applied to the piezoelectric patch bonded to one side of the slab. The patch is polarized vertically.

Numerical simulations are performed with a 3D finite element method, for a better understanding of experimental results and the related physical mechanisms. Band structures are calculated by applying Bloch boundary conditions on the lateral sides of a single unit cell or of a super-cell, depending on the distribution of rods and nuts. Transmission properties are evaluated by considering a finite PC slab as shown in Fig. 1(a). An out-of-plane wave source with unit amplitude ($U_0 = 1$) is applied on one side (S_1) of the waveguide. By sweeping the frequency, we evaluate the frequency response function (FRF) in decibel units by

$$F(f) = 20\log_{10}\left(\frac{\int_{S_2} U\mathrm{d}s}{\int_{S_1} U_0\mathrm{d}s}\right) \tag{1}$$

where U is the total displacement collected over a receiver segment (S_2) placed at the exit side of the waveguide. To differentiate the polarization of different modes, we further compute the proportion of the out-of-plane displacement in the squared total displacement via

$$p_z = \frac{\int |w|^2\mathrm{d}V}{\int (|u|^2 + |v|^2 + |w|^2)\mathrm{d}V}, \tag{2}$$

with (u, v, w) the three components of displacement in the reference frame of Figure 1(b). Experimental and numerical results are compared in detail in the following sections.

III. RESULTS AND DISCUSSION

In this section, we discuss the band structures and the frequency response of different phononic circuits.

A. Bare phononic crystal slab

For comparison, we first consider the phononic properties of the perfect PC slab summarized in Fig. 2. With

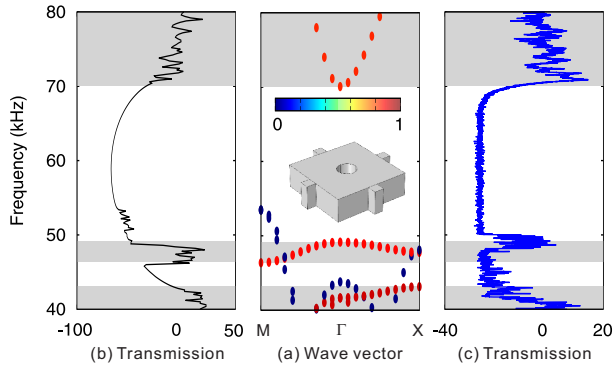

Figure 2. Band structures of the perfect PC slab (a) and transmission properties of the perfect PC obtained from simulation (b) and experiment (c). The light-gray parts mark the passing band for out-of-plane modes. The color bar represents the polarization from 0(blue) to 1(red).

the color scale in the phononic band structure varying from in-plane (blue color) to out-of-plane polarized (rd color), it is seen that both polarizations are effectively separated, as results for the mid-plane symmetry of the phononic crystal slab. Two bandgaps for out-of-plane Lamb waves are observed in the band structure, covering the frequency ranges between 43.15 and 46.37 kHz, and 49.15 kHz and 70.08 kHz. The second, larger, bandgap is mostly considered in the following. The measured frequency response is generally in agreement with the computed band structure and frequency response, though a slight upward frequency shift is observed at the entrance of the bandgap. This difference may be due to the neglection of the presence of threaded holes in the slab, effectively leading to an overestimation of the mass of the perforated lumps. Significantly, the measured bandgap is wide enough for the preparation of different waveguides operating between 50 and 70 kHz, typically.

B. Defect modes with rods and nuts

The addition of threaded rods and a pair of nuts allows one for the design of reconfigurable waveguides formed from coupled defects. We consider three different values of length l: A) $l = 0$, B) $l = 0.15a$, and C) $l = 0.3a$. The respective supercells are shown in the first column of Fig. 3. Phononic band structures are shown in the second column of the figure. As a remark, when defects are added, the structure looses the mid-plane symmetry and the separation between in-plane and out-of-plane polarized elastic waves is lost. It can be seen, however, that bands of the bare phononic crystal slab are still apparent with unchanged polarization type. Additionally, defect bands appear. Those have a color in between blue and red, meaning that their polarization is mixed and all three displacements in space coexist. Guiding bands induced by the presence of defect states are identified in dark-gray in Fig. 3. Their frequency ranges are reported in Table I.

Vibration modes around 50 kHz for defect A ($l = 0$) are shown in Fig. 3. The bottom free end of the rod vibrates in a bending motion typical of a clamped-free beam. The two modes of vibration depicted are orthogonal and couple with flexural waves of the supporting slab. Since those flexural waves are evanescent in the surrounding phononic crystal slab, the defect modes are strongly confined spatially. Globally, one of the pair of modes vibrates in the direction of the waveguide, x, whereas the other vibrates in the lateral direction, y. Given the symmetry of the excitation source with respect to the x axis in the experiment, we expect the latter mode to be deaf and hence not to be excited. In addition, another resonance appears around 65 kHz. This mode is mostly polarized out-of-plane but there is almost no coupled vibration in the rod. The displacement distribution is asymmetric with respect to the x axis, so this mode is also expected to be deaf.

When length l is increased to $0.15a$ with defect B, the vibration motion remains of the exact same type but the resonance frequency shifts upward to around 60 kHz. As argued below, the frequency shift results from the decrease in the length of the bottom free end of the rod. When length l is further increased to $0.3a$ with defect C, the resonance frequency remains almost the same, around 59 kHz. The top free end of the rod, however, is now vibrating instead of the bottom end.

As a observed above, the resonance frequency can be tuned by adjusting length l. The dynamic equation for an homogeneous rod according to Euler-Bernoulli beam theory is[38]

$$\frac{\partial^2}{\partial y^2}\left[EI\frac{\partial^2 v}{\partial y^2}\right] - \rho A\omega^2 v = 0 \qquad (3)$$

where E is Young's modulus, I is the second moment of area of the beam, and A is the cross-section area. The natural frequency for a clamped-free beam with an effective length l_e can be evaluated by

$$\omega_n = (\beta_n l_e)^2 (EI/ml_e^4)^{1/2} \qquad (4)$$

where $n = 1, 2...$ is the order of the vibration mode and $m = \rho A$ is the mass density per unit length. Numerical value for the mode constants of the first two normal modes are $(\beta_1 l_e)^2 = 3.5160$ and $(\beta_2 l_e)^2 = 22.0345$. For defect C, the resonance can be identified with the first or

Table I. Guiding bands predicted from finite element computations and measured for straight and bent waveguides. The frequency unit is kHz.

Type	A	B	C
Numerical	49.3-51.4	60.7-61.7	59.5-61.0
Straight waveguide	52.6-56.0	54.6-63.2	57.6-61.2
Bent waveguide	52.7-55.5	59.0-61.3	60.3-62.0

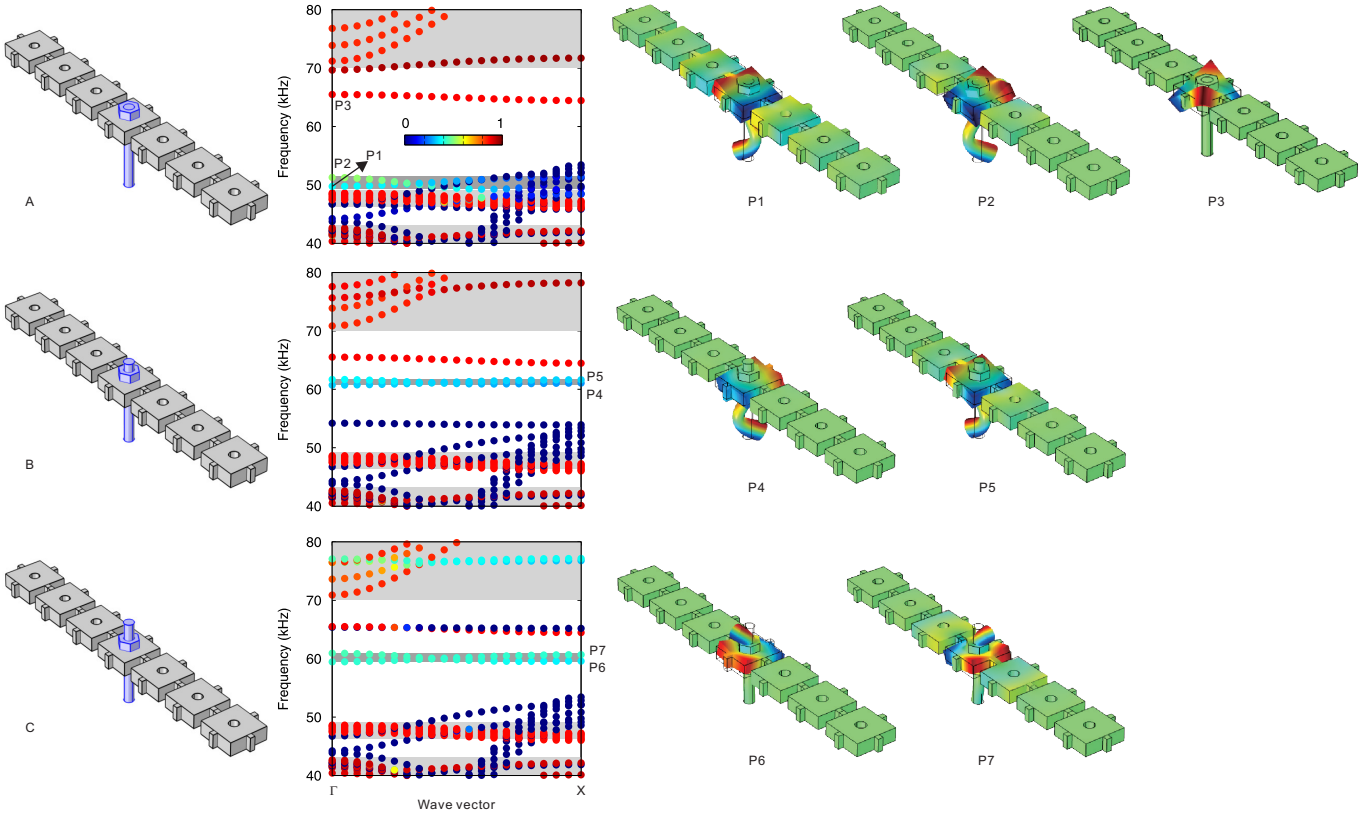

Figure 3. Phononic properties of defects composed of threaded rods held with nuts in the perforated solid phononic crystal slab of Figure 2. Three different defects are introduced, with varying value of the free length of rod l: A) $l = 0$, B) $l = 0.15a$, and C) $l = 0.3a$. In each case, the band structure for the corresponding supercell is shown. The color scale represents the contribution of out-of-plane displacements to the total polarization of elastic waves, from 0 (blue) to 1 (red). The light-gray areas indicate the passing band for the out-of-plane polarized waves in the perfect PC slab. The dark-gray areas indicate the considered waveguiding bands. Vibration modes at marked points are shown on the right. The color scale represents the normalized amplitude of out-of-plane displacements, from negative (blue) to positive (red).

fundamental normal mode, whereas for defects A and B the resonance can be identified with the second normal mode. The normal mode frequencies ω_n vary with the inverse of the square of the free length of the rod. It should be stressed, however, that the correspondence is mostly qualitative, since the nuts are not taken into account in the homogeneous beam model and the clamping boundary condition is not met since the lump deforms during vibration. Anyway, this analysis explains the continuous tunability of the resonance frequency by adjustement of the free length of the rod.

C. Straight waveguides

In this subsection, we focus on the operation of straight waveguides made from defects A, B, and C. The total length of the straight waveguides is $6a$ in the experiments, i.e. they are composed of a line of 6 defects. Numerical and experimental FRF are shown in Fig. 4. They are in fair agreement but show some differences. For all three defects, the numerical FRF predicts some transmission in a frequency band extending around 65 kHz that is not observed experimentally. From the phononic band structure, this response corresponds to mode P3 in Figure 3 that should be deaf. The numerical FRF is however quite small and may remain below the experimental detection baseline. More significant are the transmission bands highlighted in dark grey in Fig. 4. The numerical FRFs clearly correspond to the resonant frequency ranges identified in Fig. 3 and listed in Table I. The experimental FRFs appear to be shifted in frequency compared to their numerical counterparts and to have a wider frequency extension. Since it is known that the frequency bandwidth of coupled-resonator waveguides is directly related to the coupling strength between resonant defects[39], the observation indicates that coupling may be underestimated in the finite element analysis. Furthermore, clear channelled spectra are observed, with the number of maxima within transmission bands of the order of the number of defects in the coupled chain[35,40]. The frequency shifts of the resonances may be attributed to the difficulty of controlling precisely the pre-stress applied to the nuts in the experimental sample. The pre-stress is assumed to be

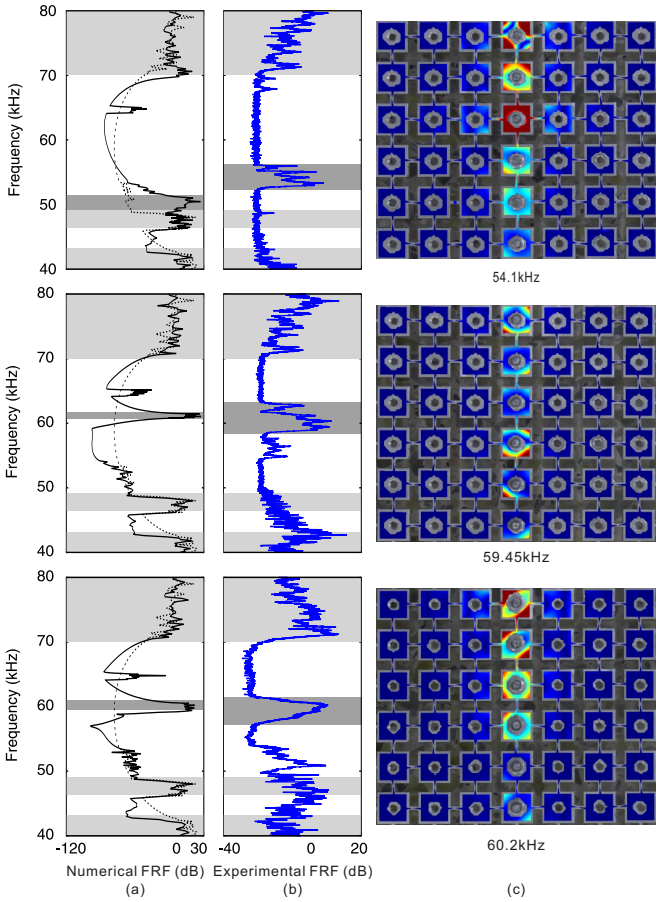

Figure 4. Frequency response function (FRF) of straight waveguides. Numerical and experimental FRFs are shown in panels (a) and (b). The light-gray areas indicate the passing bands for out-of-plane polarized waves in the perfect phononic crystal slab. The dark-gray areas indicate the waveguiding bands induced by each defect. The FRF for the bare phononic crystal slab is plotted with a dashed line in (a) for comparison. Experimentally measured displacement fields at selected frequencies are displayed in panel (c). The color-scale indicates the amplitude of out-of-plane displacement from 0 (blue) to maximum (red).

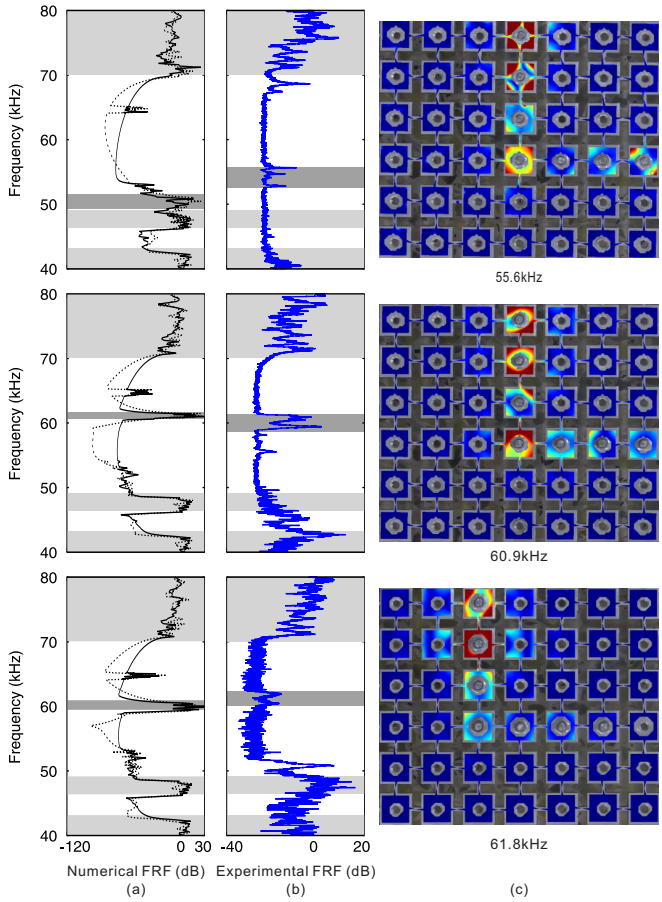

Figure 5. Frequency response function (FRF) of bent waveguides. Numerical and experimental FRFs are shown in panels (a) and (b). The light-gray areas indicate the passing bands for out-of-plane polarized waves in the perfect phononic crystal slab. The dark-gray areas indicate the waveguiding bands induced by each defect. The FRF for the bare phononic cryatl slab is plotted with a dashed line in (a) for comparison. Experimentally measured displacement fields at selected frequencies are displayed in panel (c). The colorscale indicates the amplitude of out-of-plane displacement from 0 (blue) to maximum (red).

zero in the numerical simulations. In the experiment, a varying pre-stress is probably applied to each individual defect.

Displacement fields at selected frequencies are measured over the surface and displayed in the rightmost column of Fig. 4. Vibration modes appear to be a combination of the x and y polarized modes in Fig. 3. Specifically, modes P1 and P2 degenerate for defect A, modes P4 and P5 degenerate for defect B, and modes P6 and P7 degenerate for defect C. Overall, Lamb waves are clearly guided along the waveguides at different frequencies, thus verifying the reconfigurability of the proposed system. As a note, no attempt was made at adjusting the free length of the rods to match experimental and numerical frequencies.

D. Bent waveguides

Beyond straight waveguides, the principle of coupled-resonators also allows one to design more arbitrary chains[35]. the reconfigurability principle for instance also applies to 90° bent waveguides, as we consider in this subsection. The total length of the bent waveguides is $7a$, or a chain of 7 coupled defects. Numerical and experimental FRF are shown in Fig. 5. The numerical FRFs around the resonant bands have limited changes compared to straight waveguides, although bent waveguides have an additional defect and a sharp band after the fourth defect. This observation suggests that waveguiding is very efficient in theory, and independent of the number of defects as well as of the existence of bends. The experimental FRFs show more changes, especially

regarding the width of resonant bands but also the amplitude of the response at the end of the chain of defects.

Displacement fields at selected frequencies are measured over the surface and displayed in the rightmost column of Fig. 5. As in the case of straight waveguides, the mixture of x and y polarized modes identified in Fig. 3 explains how Lamb waves are guided along the chain of defects and especially across the 90° bend.

IV. CONCLUSION

In this paper, Lamb wave propagation in phononic circuits formed by reconfigurable chains of defects has been investigated. Defects are introduced by attaching threaded rods with nuts to a two-dimensional perforated square-lattice phononic crystal slab. The consideration of threaded rods naturally provides reconfigurability by adjusting continuously their free length and hence their natural resonance frequencies. Besides, the solid phononic crystal slab is completely reusable and unaltered when reconfiguring the phononic circuits. Both straight and 90° bent waveguides were designed and fabricated. As illustrated by a simple bending cantilever model, the central frequency can span the available complete phononic band gap. In numerical simulations, the frequency response function is almost independent of the length of the chain of defects and of the presence of bends. Experimental results are generally in fair agreement with numerical ones, though the mechanical reconfigurablility provided by a human experimenter remains somehow imprecise, including the pre-stress applied when fastening the nuts. Mechanical robots with force sensors may be considered to conduct precise control of wave propagation. Other phononic circuits could also be designed as a direct extension of the present work.

ACKNOWLEDGMENTS

Financial support by the National Natural Science Foundation of China (12021002, 11991031, and 11991032) is gratefully acknowledged. VL acknowledges support by the EIPHI Graduate School (contract "ANR-17-EURE-0002").

DATA AVAILABILITY

The data that support the findings of this study are available from the corresponding authors upon reasonable request.

REFERENCES

[1]M. S. Kushwaha, P. Halevi, L. Dobrzyński, and B. Djafari-Rouhani, "Acoustic band structure of periodic elastic composites," Physical Review Letters **71**, 2022 (1993).

[2]M.-B. Assouar, M. Senesi, M. Oudich, M. Ruzzene, and Z.-L. Hou, "Broadband plate-type acoustic metamaterial for low-frequency sound attenuation," Applied Physics Letters **101**, 173505 (2012).

[3]A. Khelif, A. Choujaa, S. Benchabane, B. Djafari-Rouhani, and V. Laude, "Guiding and bending of acoustic waves in highly confined phononic crystal waveguides," Applied Physics Letters **84**, 4400 (2004).

[4]Y. Pennec, B. Djafari-Rouhani, J. O. Vasseur, A. Khelif, and P. A. Deymier, "Tunable filtering and demultiplexing in phononic crystals with hollow cylinders," Physical Review E **69**, 046608 (2004).

[5]Y. Pennec, B. Djafari-Rouhani, J. O. Vasseur, H. Larabi, A. Khelif, A. Choujaa, S. Benchabane, and V. Laude, "Acoustic channel drop tunneling in a phononic crystal," Applied Physics Letters **87**, 261912 (2005).

[6]M. I. Hussein, M. J. Leamy, and M. Ruzzene, "Dynamics of phononic materials and structures: Historical origins, recent progress, and future outlook," Applied Mechanics Reviews **66**, 040802 (2014).

[7]Y.-F. Wang, Y.-Z. Wang, B. Wu, W. Chen, and Y.-S. Wang, "Tunable and active phononic crystals and metamaterials," Applied Mechanics Reviews **72**, 040801 (2020).

[8]V. Laude, *Phononic Crystals: Artificial Crystals for Sonic, Acoustic, and Elastic Waves* (Walter de Gruyter GmbH, Berlin, 2015).

[9]R. Zhu, Y.-Y. Chen, M. V. Barnhart, G.-K. Hu, C.-T. Sun, and G.-L. Huang, "Experimental study of an adaptive elastic metamaterial controlled by electric circuits," Applied Physics Letters **108**, 011905 (2016).

[10]K.-L. Jim, C.-W. Leung, S.-T. Lau, S.-H. Choy, and H.-L.-W. Chan, "Thermal tuning of phononic bandstructure in ferroelectric ceramic/epoxy phononic crystal," Applied Physics Letters **94**, 193501 (2009).

[11]J. F. Robillard, O. B. Matar, P. A. Vasseur, J. O.and Deymier, M. Stippinger, A. C. Hladky-Hennion, Y. Pennec, and B. Djafari-Rouhani, "Tunable magnetoelastic phononic crystals," Applied Physics Letters **95**, 124104 (2009).

[12]S. W. Xiao, G. C. Ma, Y. Li, Z. Y. Yang, and P. Sheng, "Active control of membrane-type acoustic metamaterial by electric field," Applied Physics Letters **106**, 091904 (2015).

[13]W. Qian, Z.-Y. Yu, X.-L. Wang, Y. Lai, and B.-B. Yellen, "Elastic metamaterial beam with remotely tunable stiffness," Journal of Applied Physics **119**, 055102 (2016).

[14]O. R. Bilal, A. Foehr, and C. Daraio, "Reprogrammable phononic metasurfaces," Advanced Materials **18**, 1700628 (2017).

[15]J.-H. Oh, I. K. Lee, P. S. Ma, and Y.-Y. Kim, "Active wave-guiding of piezoelectric phononic crystals," Applied Physics Letters **99**, 083505 (2011).
[16]Y.-Z. Wang, F.-M. Li, and Y.-S. Wang, "Active feedback control of elastic wave metamaterials," Intelligent Material Systems and Structures **28**, 2110 (2017).
[17]F. Casadei, T. Delpero, A. Bergamini, P. Ermanni, and M. Ruzzene, "Piezoelectric resonator arrays for tunable acoustic waveguides and metamaterials," Journal of Applied Physics **112**, 064902 (2012).
[18]H. Pichard, O. Richoux, and J.-H. Groby, "Experimental demonstrations in audible frequency range of band gap tunability and negative refraction in two-dimensional sonic crystal," Journal of the Acoustical Society of America **132**, 2816 (2012).
[19]Y. Jin, Y. Pennec, Y.-D. Pan, and B. Djafari-Rouhani, "Phononic crystal plate with hollow pillars actively controlled by fluid filling," Crystals **6**, 64 (2016).
[20]T.-T. Wang, Y.-F. Wang, Y.-S. Wang, and V. Laude, "Tunable fluid-filled phononic metastrip," Applied Physics Letters **111**, 041906 (2017).
[21]Y.-F. Wang, T.-T. Wang, Y.-S. Wang, and V. Laude, "Reconfigurable phononic crystal circuits formed by coupled acoustoelastic resonators," Physical Review Applied **8**, 014006 (2017).
[22]T. Mullin, S. Deschanel, K. Bertoldi, and M. C. Boyce, "Pattern transformation triggered by deformation," Physical Review Letters **99**, 084301 (2007).
[23]B. Li, Y.-P. Cao, X.-Q. Feng, and H. Gao, "Mechanics of morphological instabilities and surface wrinkling in soft materials: A review," Soft Matter **8**, 5728 (2012).
[24]P. Wang, F. Casadei, S. Shan, J. C. Weaver, and K. Bertoldi, "Harnessing buckling to design tunable locally resonant acoustic metamaterials," Physical Review Letters **113**, 014301 (2014).
[25]S. Shan, S. H. Kang, P. Wang, C. Qu, S. Shian, E. R. Chen, and K. Bertoldi, "Harnessing multiple folding mechanisms in soft periodic structures for tunable control of elastic waves," Advanced Functional Materials **24**, 4935 (2014).
[26]A. Bayat and F. Gordaninejad, "A thermally tunable phononic crystal," in *Proceedings of the Behavior and Mechanics of Multifunctional Materials and Composites* (2016).
[27]M. Ruzzene and A. Baz, "Control of wave propagation in periodic composite rods using shape memory inserts," Journal of Vibration and Acoustics **122**, 151 (2000).
[28]T.-T. Wu, J.-C. Hsu, and J.-H. Sun, "Phononic plate waves," IEEE Transcations on Ultrasonics, Ferroelectrics, and Frequency Control **58**, 2146–2161 (2011).
[29]A. Climente, D. Torrent, and J. Sánchez-Dehesa, "Gradient index lenses for flexural waves based on thickness variations," Applied Physics Letters **105**, 064101 (2014).
[30]M. Miniaci, A. Marzani, N. Testoni, and L. D. Marchi, "Complete band gaps in a polyvinyl chloride (pvc) phononic plate withcross-like holes: numerical design and experimental verification," Ultrasonics **56**, 251–259 (2015).
[31]Y.-F. Wang and Y.-S. Wang, "Multiple wide complete bandgaps of two-dimensional phononic crystal slabs with cross-like holes," Journal of Sound and Vibration **332**, 2019–2037 (2013).
[32]F.-L. Hsiao, A. Khelif, H. Moubchir, A. Choujaa, C.-C. Chen, and V. Laude, "Waveguiding inside the complete band gap of a phononic crystal slab," Physical Review E **76**, 056601 (2007).
[33]M. Oudich, M. B. Assouar, and Z.-L. Hou, "Propagation of acoustic waves and waveguiding in a two-dimensional locally resonant phononic crystal plate," Applied Physics Letters **97**, 193503 (2010).
[34]Y. Xiao, J.-H. Wen, and X.-S. Wen, "Flexural wave band gaps in locally resonant thin plates with periodically attached spring-mass resonators," Journal of Physics D: Applied Physics **45**, 195401 (2012).
[35]T.-T. Wang, S. Bargiel, F. Lardet-Vieudrin, Y.-F. Wang, Y.-S. Wang, and V. Laude, "Collective resonances of a chain of coupled phononic microresonators," Physical Review Applied **13**, 014022 (2020).
[36]Y.-F. Wang, T.-T. Wang, J.-P. Liu, Y.-S. Wang, and V. Laude, "Guiding and splitting lamb waves in coupled-resonator elastic waveguides," Composite Structures **206**, 588–593 (2018).
[37]H. Zhu and F. Semperlotti, "Metamaterial based embedded acoustic filters for structural applications," AIP Advances (2013).
[38]W. T. Thomson, *Theory of vibration with application* (Prentice-Hall, New Jersey, 1983).
[39]J. M. Escalante, A. Martínez, and V. Laude, "Dispersion relation of coupled-resonator acoustic waveguides formed by defect cavities in a phononic crystal," Journal of Physics D: Applied Physics **46**, 475301 (2013).
[40]Y.-F. Wang, T.-T. Wang, J.-W. Liang, Y.-S. Wang, and V. Laude, "Channeled spectrum in the transmission of phononic crystal waveguides," Journal of Sound and Vibration **437**, 410–421 (2018).